

TYPE I MIGRATION IN A NON-ISOTHERMAL PROTOPLANETARY DISK

HANNAH JANG-CONDELL¹ AND DIMITAR D. SASSELOV
Harvard-Smithsonian Center for Astrophysics
60 Garden St., Cambridge, MA 02138(Received May 5, 2004; Revised September 28, 2004; Accepted October 8, 2004)
To appear in the Astrophysical Journal

ABSTRACT

We calculate rates of Type I migration of protoplanets in a non-isothermal three-dimensional protoplanetary disk, building upon planet-disk models developed in previous work. We find that including the vertical thickness of the disk results in a decrease in the Type I migration rate by a factor of ~ 2 from a two-dimensional disk. The vertical temperature variation has only a modest effect on migration rates since the torques at the midplane are weighted heavily both because the density and the perturbing potential are maximized at the midplane. However, temperature perturbations resulting from shadowing and illumination at the disk's surface can decrease the migration rate by up to another factor of 2 for planets at the gap-opening threshold at distances where viscous heating is minimal. This would help to resolve the timescale mismatch between the standard core-accretion scenario for planet formation and the survival of planets, and could help explain some of the rich diversity of planetary systems already observed.

Subject headings: planetary systems: formation — planetary systems: protoplanetary disks — accretion disks

1. INTRODUCTION

The issue of planetary migration due to tidal interactions between the planet and a circumstellar disk was first addressed by Goldreich & Tremaine (1980), who found that the potential of an orbiting planet excites Lindblad resonances in the disk, resulting in the transfer of angular momentum. They found that the resulting torques on the planet are similar in magnitude, so that whether the planet moves inward or outward from angular momentum exchange depends on how the torques from the inner and outer disk balance out. Ward (1986) found that given a decreasing radial temperature profile, the torques from the outer disk are greater than those from the inner disk, resulting in a net torque that forces the planet inward. Planetary migration via this mechanism is referred to as Type I migration to distinguish it from Type II migration, which is the radial drift of planets massive enough to clear all material out of the Lindblad resonances, thereby forming a gap in the disk and moving together with the disk as it is accreted onto the star (Ward 1997a).

Subsequent work on two-dimensional disks confirms the prediction that planets in protoplanetary disks migrate inward on short timescales on the order of $\lesssim 10^5$ yr for Earth mass planets (e.g., Artymowicz 1993a; Korycansky & Pollack 1993; Ward 1997a). Tanaka et al. (2002, hereafter TTW) find that including the three-dimensional density structure of an isothermal disk increases the migration timescale by a factor of 2 or 3 over a two-dimensional calculation. Menou & Goodman (2004) calculate migration rates in a disk with a radial temperature profile expected in T Tauri disks and also find that the migration timescales increase when the thickness of the disk is accounted for. In a disk model that includes MHD turbulence, the density fluctuations near the planet can be sufficient to change the magnitude and even the sign of the total net torque on a small planet, so that the planet migrates as a “random walk” rather than a steady inward drift

(Nelson & Papaloizou 2004).

While the effect of the density structure in the vicinity of a protoplanet on its migration rate has been studied in detail both analytically and in numerical simulations, the effect of local temperature variations has not (e.g., Kley 1999; Kley et al. 2001; Bate et al. 2003). Most simulations of planets embedded in disks employ a vertically isothermal equation of state, so that the disk has a simple radially dependent temperature structure. Similarly, the analytic calculations discussed above assume vertical isothermality for simplicity. In this paper, we analyze Type I migration torques from Lindblad resonances in a protoplanetary disk where viscous heating and stellar illumination are the primary heating sources. Further, we examine how temperature variations induced by the presence of the planet itself affect Type I migration.

Disk temperature variations can affect the net Lindblad torques by changing the local pressure gradient in the disk. A pressure gradient shifts the angular frequency of the gas orbiting the star with respect to Keplerian velocities, which in turn shifts the positions of the Lindblad resonances (Ward 1997a). The forcing function depends on the distance to the planet, so the torques on the planet vary with the locations of the Lindblad resonances. To date, no one has addressed how a non-isothermal temperature structure will affect the magnitude of the angular momentum transferred at the Lindblad resonances and how that might affect migration rates. A variation in temperature structure, such as those described in Jang-Condell & Sasselov (2003, hereafter Paper I) and Jang-Condell & Sasselov (2004, hereafter Paper II), due to radiative transfer effects, may affect the balance of migration torques.

In this paper, we address how the temperature structure of the disk affects the locations of Lindblad resonances and the consequences for Type I migration. In §2 we derive the equations used for calculating the torques on the planet from Lindblad resonances in a non-isothermal disk. In §3 we describe our adopted model disk and briefly discuss how the presence of a planet changes the temperature structure of the disk. We present our results in §4 and discuss their implications in §5.

¹ Now at the Carnegie Institution of Washington, Department of Terrestrial Magnetism, 5241 Broad Branch Rd., NW, Washington, DC 20015
Electronic address: hannah@dtm.ciw.edu

Finally, in §6 we present our conclusions.

2. TORQUES AT LINDBLAD RESONANCES

In a two-dimensional disk, only one wave mode is excited at each Lindblad resonance. In a three-dimensional disk, vertical velocity perturbations are allowed, so an entire series of wave modes is excited at each Lindblad resonance (TTW, Takeuchi & Miyama 1998; Lubow & Ogilvie 1998). The lowest wave mode, referred to as the $n = 0$ mode in TTW and the f -mode in Lubow & Ogilvie (1998), has no vertical velocity component in a vertically isothermal disk, so it is often referred to as the two-dimensional wave mode. This corresponds to the wave that is excited in the two-dimensional disk, although its properties are somewhat different since it is propagated through a disk with a finite height instead of an infinitesimally thin disk. The bulk of the angular momentum, even in thermally stratified disks, is carried by the two-dimensional wave (Lubow & Ogilvie 1998), so we shall concentrate our analysis on this wave mode. Vertical motions do occur in a thermally stratified disk, but we assume that these are small compared to the horizontal velocity perturbations. As it is the total angular momentum that the wave carries that interests us, the exact form of the wave propagation is outside the scope of this paper.

The pressure gradient is important in the calculation of relative torques because it determines the location of the resonances, indirectly contributing to the magnitude of the torque. Local temperature variations can shift the locations of the Lindblad resonances by changing the local pressure gradient. This so-called pressure buffer can significantly affect the total net torques from Lindblad resonances (Ward 1997a). We assume that the density ρ and temperature T are not necessarily constant with either radius or height, therefore the pressure p and sound speed c vary locally as well.

2.1. Resonance Locations

Euler's equation for the unperturbed disk is

$$\frac{\partial \mathbf{v}}{\partial t} + (\mathbf{v} \cdot \nabla) \mathbf{v} = -\frac{1}{\rho} \nabla p - \nabla \left(-\frac{GM_*}{|\mathbf{r}|} \right), \quad (1)$$

where we adopt an ideal gas equation of state so that $p = \rho c^2 = \rho kT / \mu m_H$ where k is the Boltzmann constant, μ is the mean molecular weight ($\mu = 2$ for molecular hydrogen), and m_H is an atomic mass unit. We adopt a cylindrical coordinate system, $\mathbf{r} = (r, \theta, z)$ where r is the distance from the z -axis and θ is the azimuthal angle. Assuming that the gas in the disk travels in circular orbits with $\mathbf{v} = r\Omega\hat{\theta}$, then the radial component of equation (1) becomes

$$r\Omega^2 = \frac{1}{\rho} \frac{\partial p}{\partial r} + \frac{GM_*}{r^2(1+z^2/r^2)^{3/2}} \quad (2)$$

where G is the gravitational constant, and M_* is the mass of the star. The equation for the angular velocity of the disk is

$$\Omega^2 = \Omega_K^2 \left(1 + \frac{z^2}{r^2} \right)^{-3/2} + \frac{c^2}{r^2} \left(\frac{\partial \log p}{\partial \log r} \right) \quad (3)$$

where $\Omega_K = \sqrt{GM_*/r}$. Defining $k \equiv -\partial \log \rho / \partial \log r$, $l \equiv -\partial \log p / \partial \log T$, and $h \equiv c/\Omega_K$, we can rewrite equation (3) as

$$\Omega^2 = \Omega_K^2 \left[1 - \frac{h^2}{r^2} \left(\frac{3z^2}{2h^2} + k + l \right) \right], \quad (4)$$

omitting terms of $\mathcal{O}(z^4/r^4)$ and higher. This equation differs from calculations of the angular velocity in two-dimensional disks which use integrated quantities in that Ω varies with disk height (e.g., Ward 1997a). If $k_\sigma = -\partial \log \sigma / \partial \log r$ where $\sigma = \int_{-\infty}^{\infty} \rho dz$ is the surface density, then in general, $k \neq k_\sigma$. In the example of a vertically isothermal disk where $\rho = \frac{\sigma}{\sqrt{2\pi}h} \exp(-z^2/2h^2)$, the density gradient is

$$k = k_\sigma + \left(\frac{z^2}{h^2} - 1 \right) \left(\frac{l}{2} - \frac{3}{2} \right), \quad (5)$$

which yields

$$\Omega^2 = \Omega_K^2 \left\{ 1 - \frac{h^2}{r^2} \left[\frac{3}{2} + k_\sigma + \frac{l}{2} \left(\frac{z^2}{h^2} + 1 \right) \right] \right\} \quad (6)$$

as in TTW. The angular velocity is constant with z only in an isothermal disk, where $l = 0$. Realistic protoplanetary disk models, however, are not isothermal.

We now consider a planet orbiting the star in the plane of the disk at $r = a$ and with angular velocity $\Omega_p = \sqrt{GM_*/a}$. The effective location of the m th order Lindblad resonance is where r satisfies

$$D_* \equiv \kappa^2 - m^2(\Omega - \Omega_p)^2 + (mc/r)^2 = 0 \quad (7)$$

where κ is the local epicycle frequency of the disk,

$$\kappa = \frac{1}{r^3} \frac{\partial}{\partial r} (r^4 \Omega^2) \quad (8)$$

(Artymowicz 1993b; Ward 1988, 1997a). We assume that $\kappa \approx \Omega$, since the departure from a Keplerian flow is small, and we find that using equation (8) to solve exactly for κ yields very similar results for the resonance positions and torques. Defining $\xi = mc/r\kappa$, then

$$\frac{\Omega_p}{\Omega} = 1 + \frac{\epsilon}{m} \sqrt{1 + \xi^2} \quad (9)$$

where

$$\epsilon = \begin{cases} +1, & \text{for outer resonances} \\ -1, & \text{for inner resonances.} \end{cases} \quad (10)$$

Then we can solve for the location of the Lindblad resonance, $\alpha_r = r/a$, as

$$\alpha_r^{3/2} = \left[1 + \frac{\epsilon}{m} \sqrt{1 + \xi^2} \right] \left(\frac{\Omega}{\Omega_K} \right). \quad (11)$$

We solve for α_r and ξ iteratively using equations (4) and (11), as in Ward (1997a). The iteration is necessary because the magnitude of the torque is sensitive to the precise position of the resonance. Simply calculating α_r to first order in h/r can introduce a systematic shift in the resonance positions which will affect the overall balance of torques.

2.2. Disk Torque Strength

In a two-dimensional disk, the magnitude of the torque exerted near the m th order Lindblad resonance is

$$T_m = -\frac{\pi^2 m \sigma \Psi_m^2}{r d D_*/dr} \quad (12)$$

where σ is the unperturbed surface density of the disk. The forcing function of the planet, Ψ_m , is defined by Ward (1997a) to be

$$\Psi_m = \frac{rd\phi_m/dr + 2mf\phi_m}{\sqrt{1+4\xi^2}}, \quad (13)$$

where $f = m(\Omega - \Omega_p)/\Omega$, and ϕ_m is the amplitude of the m th order Fourier component of the disturbing function,

$$\phi_m = -\frac{Gm_p}{a} b_{1/2}^m(\alpha_r) \quad (14)$$

where $b_{1/2}^m(\alpha_r)$ is known as the Laplace coefficient, defined as

$$b_{1/2}^m(\alpha_r) = \frac{2}{\pi} \int_0^\pi \frac{\cos m\theta d\theta}{\sqrt{1-2\alpha_r \cos \theta + \alpha_r^2}}. \quad (15)$$

At the effective location of the Lindblad resonance, $f = -\epsilon\sqrt{1+\xi^2}$.

To truly calculate the torques at Lindblad resonances in a three-dimensional disk requires a solution to the linearized fluid equations in three dimensions. For a polytropic or isothermal equation of state, the eigenmodes can be solved for directly; these cases have been studied by others (Lubow & Ogilvie 1998, TTW). The temperature structure of the disk calculated in our model is neither polytropic nor isothermal, so we require a numerical solution. To simplify the problem, we assume that the vertical velocity perturbations are small compared to the horizontal ones so that we can treat the disk as the sum of independent layers and add up the total torque from these layers, as suggested by Ward (1988) and Artymowicz (1993b). This relies on the assumption that relatively little angular momentum is carried away by vertical velocity perturbations, so our calculations should be treated as a useful estimate of the three-dimensional Lindblad resonant torque rather than a rigorous solution.

For a disk with vertical extent, the forcing function must be modified to account for the vertical averaging of the planet potential's disturbing function. We can express the torque on the disk at height z over an extent dz as

$$d\tilde{T}_m = -\frac{\pi^2 m \rho \tilde{\Psi}_m^2}{r dD_*/dr} dz \quad (16)$$

where ρ , r and D_* are evaluated at the location of the Lindblad resonance at height z given the temperature structure at that height, and $\tilde{\Psi}_m$ is calculated with a modified Laplace coefficient

$$b_{1/2}^m(\alpha_r, \zeta) = \frac{2}{\pi} \int_0^\pi \frac{\cos m\theta d\theta}{\sqrt{1-2\alpha_r \cos \theta + \alpha_r^2 + \zeta^2}} \quad (17)$$

where $\zeta = z/r$.

As noted in Goldreich & Tremaine (1980), for $|\alpha_r - 1| \ll 1$ and $m \gg 1$, most of the contribution to the integral comes from $\theta \ll 1$. In other words, local conditions around the planet have the most effect on angular momentum transfer at Lindblad resonances. This is because most of the angular momentum transfer occurs from close encounters between gas streamlines and the planet. We can then approximate the Laplace coefficient by replacing $\cos \theta$ with $1 - \theta^2/2$ and extending the upper limit of the integral to infinity. Then,

$$b_{1/2}^m(\alpha_r, \zeta) \approx \frac{2}{\pi \sqrt{\alpha_r}} \int_0^\infty \frac{\cos \theta d\theta}{\sqrt{m^2[(1-\alpha_r)^2 + \zeta^2]/\alpha_r + \theta^2}} = \frac{2}{\pi \sqrt{\alpha_r}} K_0(\Lambda) \quad (18)$$

where K_i is the modified Bessel function of order i and

$$\Lambda = m \sqrt{\frac{(\alpha_r - 1)^2 + \zeta^2}{\alpha_r}}. \quad (19)$$

Making use of the relation $K'_0 = -K_1$ (Abramowitz & Stegun 1972),

$$\begin{aligned} \frac{r}{GM_*/a} \frac{d\phi_m}{dr} &= -\alpha_r \frac{db_{1/2}^m}{d\alpha_r} \\ &= \frac{1}{\pi} \left\{ \frac{K_0(\Lambda)}{\sqrt{\alpha_r}} + \frac{m[\alpha_r^2 - \zeta^2 - 1]K_1(\Lambda)}{\alpha_r \sqrt{(\alpha_r - 1)^2 + \zeta^2}} \right\}. \end{aligned} \quad (20)$$

We define a dimensionless forcing function

$$\begin{aligned} \psi_m &\equiv \frac{\epsilon \pi}{2m} \frac{a}{GM_*} \sqrt{1+4\xi^2} \tilde{\Psi}_m \\ &= \frac{\pi}{2} \left[-\epsilon \frac{\alpha_r}{m} \frac{db_{1/2}^m(\alpha_r, \zeta)}{d\alpha_r} + 2\sqrt{1+\xi^2} b_{1/2}^m(\alpha_r, \zeta) \right]. \end{aligned} \quad (21)$$

Substituting in the Bessel function formulation of $b_{1/2}^m(\alpha_r, \zeta)$,

$$\psi_m = \frac{\epsilon(\alpha_r^2 - \zeta^2 - 1)}{2\alpha_r \sqrt{(\alpha_r - 1)^2 + \zeta^2}} K_1(\Lambda) + \left(\frac{\epsilon}{2m} + 2m\sqrt{1+\xi^2} \right) \frac{K_0(\Lambda)}{\sqrt{\alpha_r}}. \quad (22)$$

When $\zeta = 0$, this equation reduces to the forcing function calculated by Ward (1997a) for a two-dimensional disk.

The total torque integrated over the vertical extent of the disk is then

$$\tilde{T}_m = \frac{\pi^2 m}{r dD_*/dr} \int_{-\infty}^{\infty} \rho \tilde{\Psi}_m^2 dz. \quad (23)$$

If we assume that the transferred angular momentum is entirely dissipated in the disk, then the net torque exerted by the planet on the disk for the m th order inner and outer Lindblad resonances is

$$\Gamma_m = \tilde{T}_m^{\text{outer}} - \tilde{T}_m^{\text{inner}} \quad (24)$$

and the total torque is

$$\Gamma_{\text{tot}} = \sum_{m>1} \Gamma_m. \quad (25)$$

When Γ is positive (negative), the planet loses (gains) angular momentum, and the planet migrates inward (outward).

2.3. Migration Rates

Since we consider planets at or below the gap-opening threshold, we assume that the torques exerted on the disk by the planet are entirely dissipated in the disk and that the torque of the disk on the planet is equal to the torques from the planet on the disk. We do not take into account the changes to the disk made by the action of the tidal torques. We expect that in general, the effect of the torques will be to decrease the density of the nearby disk by pushing material out of the Lindblad resonances so our torque estimates are upper limits. In the absence of feedback from the disk, the rate of change in the planet's angular momentum is equal to the total torque, and the rate at which the planet moves is

$$\frac{da}{dt} = -\frac{2\Gamma_{\text{tot}}}{m_p a \Omega_p}. \quad (26)$$

Negative values of da/dt indicate inward migration, positive values indicate outward migration. The migration timescale is

$$t_m = \frac{m_p \Omega_p}{|2\Gamma_{\text{tot}}|} \quad (27)$$

3. DISK MODEL

The model disk is described in detail in Paper II, both with and without planets. In this section we will summarize the features of the model disk and the temperature changes caused by the presence of planets. When calculating the positions and torque strengths of the Lindblad resonances, we do not take into account the response of the disk to torques from the planets. In particular, we do not address density perturbations in the disk such as spiral density waves or gap-clearing for the larger planets in our models. These density modifications will affect both the locations of the resonances as well as the magnitude of the torques, but that calculation is outside the scope of this paper.

3.1. The Unperturbed Disk

To calculate the unperturbed disk structure, we adopt the formalism developed by Calvet et al. (1991) and D'Alessio et al. (1998, 1999), with some simplifying assumptions. The model we employ is one of a gaseous disk rotating around a hot young star where dust is the primary opacity source, and the gas and dust are well mixed. The star is no longer actively accreting and has no outflow, so the disk is quiescent. The star has temperature T_* = 4000 K, radius R_* = 2 R_\odot , and mass M_* = 0.5 M_\odot . The disk is accreting at $\dot{M} = 10^{-8} M_\odot \text{ yr}^{-1}$ and has a Shakura-Sunyaev viscosity parameter of $\alpha_{\text{SS}} = 0.01$ (Shakura & Sunyaev 1973).

To find the temperature structure of the model disk, we calculate radiative transfer through the disk with two heat sources: viscous heating and stellar irradiation. Figure 1 summarizes the resulting vertical temperature and density profiles. The upper and lower panels of each plot shows the temperature and density, respectively, of the disk versus scale height at 0.5, 1, 2, and 4 AU. The dotted line in the lower panels show the density profile for a vertically isothermal disk with the same midplane temperature and surface density for comparison. The vertical line in each plot indicates the location of the photosphere, where the optical depth of the disk is 2/3. Viscous heating is dissipated at the midplane, so the temperature decreases with increasing z . Stellar irradiation at the surface creates a temperature inversion, where the uppermost layers are hotter than lower layers. The photosphere is approximately the location of the vertical temperature minimum.

The viscous temperature goes as $r^{-3/4}$ while the stellar radiation temperature goes as $r^{-1/2}$, so that close to the star, viscous heating dominates. This causes the midplane temperature to be much higher than even the surface temperature at small r . Conversely, at larger radii the midplane temperature becomes close to the photosphere temperature.

3.2. Disk with a Planet – Spatial Temperature Variations

When we insert a planet into the model disk, its gravitational potential induces a compression of the disk material near it, resulting in a decrement in the density at the disk's surface. Thus, an isodensity contour at the height of the photosphere takes on the shape of a well. When this well is illuminated by stellar irradiation at grazing incidence, it results in cooling in a shadowed region and heating in an exposed region.

The temperature variations caused by shadowing and illumination effects can change the local pressure gradient, which will in turn shift the locations of the Lindblad resonances. As noted in §2.2, the integral for the perturbing potential is

weighted toward $\theta \ll 1$ for $|\alpha_r - 1| \ll 1$ and $m \gg 1$, implying that disk properties immediately around the planet have the most effect on angular momentum transfer at Lindblad resonances. Although the equations for calculating torques at Lindblad resonances assume an axisymmetric disk structure, we can set quantities such as density and temperature equal to the local values rather than azimuthally averaged quantities.

In order to quantify the effect of temperature variations on Lindblad torques, we extract the temperature structure through a slice of the planet-disk models calculated in Paper II, perpendicular to the planet's orbit and through the position of the planet and use this to determine the perturbed pressure gradient near the planet. This yields new values for the tidal torques on the disk, and correspondingly different migration rates. Our calculations are meant to put limits on the effect temperature variations from radiative transfer effects might have on migration rates of planets embedded in disks.

We use a spline interpolation to calculate the temperature between the gridded points, since we want both T and dT/dr to be continuous and smooth. Since the density structure within about r_H of the planet is not well described because this material is being accreted onto the planet, the temperature structure in this region is also not well understood in our models. For this reason, we assume that the temperature simply varies linearly across the region within r_H from the planet. This assumption does not significantly affect the calculation of the tidal torques, since the effective resonance locations are at $|r-a| \gtrsim 2h/3$.

4. RESULTS

In Paper II, we calculated the three-dimensional temperature structure around planets embedded in protoplanetary disks, taking shadowing and illumination effects at the surface of the disk into account. We shall put limits on the effect that these temperature variations can have on migration by taking a radial slice through the calculated volume at the planet's position and finding the migration rates associated with these temperature profiles. We calculate the torques at the Lindblad resonances and integrate in z from the midplane to the photosphere. Note that the photosphere is typically about twice the scale height of the disk above the midplane. Above the photosphere, the disk is very rarefied, more than an order of magnitude less in density, so contributions to the total torque are not significant.

Figure 2 summarizes the total net torques calculated for varying planet masses at several distances: crosses for 0.5 AU, triangles for 1 AU, squares for 2 AU, and stars for 4 AU. The torque is normalized to

$$\Gamma_0 = \left(\frac{m_p}{M_*} \right)^2 \sigma_0 a^4 \Omega_p^2. \quad (28)$$

Note that this quantity incorporates the scaling with both stellar and planetary masses. The solid lines show the torques for the unperturbed model disk, and the dotted lines indicate the torques for a vertically isothermal disk with the same integrated surface density with temperature equal to that at the midplane. The dashed lines show how the total net torque varies with planet mass when we include the temperature variations from radiative transfer.

In order to better understand how temperature perturbations alter migration torques, we discuss how the torque on the disk

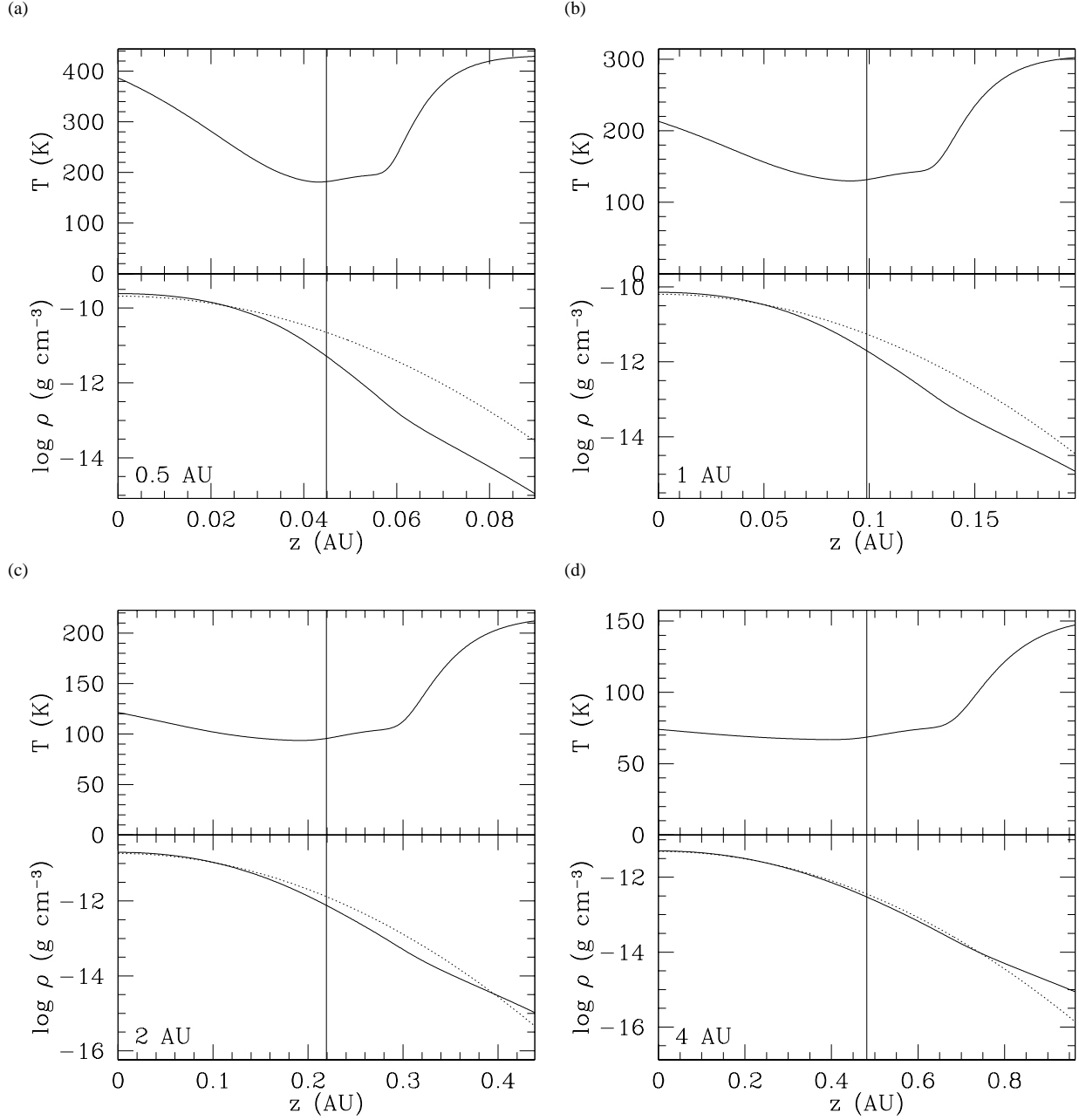


FIG. 1.— Vertical temperature and density profiles of the unperturbed disk at (a) 0.5, (b) 1, (c) 2, and (d) 4 AU. The vertical line in each plot shows the location of the photosphere. The dotted line shows the density profile of a vertically isothermal disk at the temperature of the midplane with the same surface density for comparison.

varies with z . Noting that

$$\Gamma_{\text{tot}} = \sum_{m>1} \int_{-\infty}^{\infty} \left(\frac{d\tilde{T}_m^{\text{outer}}}{dz} - \frac{d\tilde{T}_m^{\text{inner}}}{dz} \right) dz \quad (29)$$

we define the scaled torque density as

$$\gamma(z) = \frac{\sigma_0}{\rho} \frac{d\Gamma_{\text{tot}}}{dz} = \frac{\sigma_0}{\rho} \sum_{m>1} \frac{d\tilde{T}_m^{\text{outer}}}{dz} - \frac{d\tilde{T}_m^{\text{inner}}}{dz} \quad (30)$$

Since $\gamma(z)$ is scaled by σ_0 , this quantity has the units of torque.

We plot the scaled torque density in terms of Γ_0 versus z at 1, 2, and 4 AU in the upper panels of Figures 3, 4 and 5, respectively. In each plot, the vertical line indicates the

scale height of the disk, $h_0 = c_0/a\Omega_p$ where c_0 is the sound speed at the midplane of the disk. The short lines on the left edge of the plot show the total integrated torque in terms of Γ_0 for the unperturbed model disk (*solid line*) and a vertically isothermal model (*dashed line*). The line labeled “2D” shows total net torque predicted for a two-dimensional disk with the same surface density profile as the model disk, and temperature given by the midplane of the disk. Note that this value is almost exactly equal to the value of the scaled torque density at the midplane for a disk with no planet. The solid lines indicate the torque density profiles for the disk with temperature perturbations induced by planets of varying mass, as labeled on the plot. The topmost line, labelled $0 M_{\oplus}$, shows the scaled

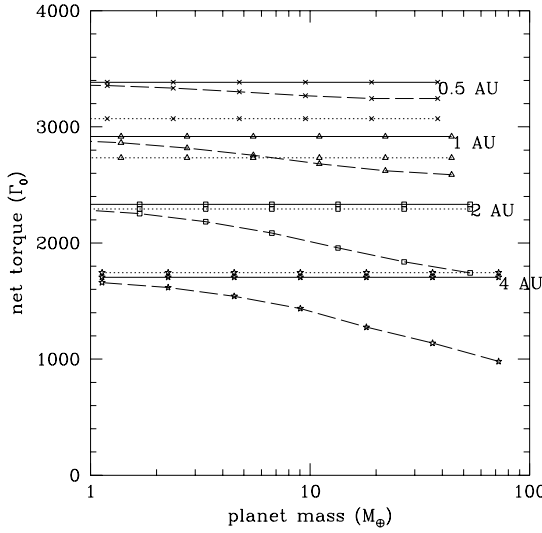


FIG. 2.— Total net torques at 0.5 (crosses), 1 (triangles), 2 (squares) and 4 (stars) AU. The solid lines indicate the total net torque for the unperturbed model disk and the dotted lines indicate the total net torque for an isothermal disk at the midplane temperature. The dashed lines indicate the total net torque for the model disk with a planet of the mass indicated by the horizontal axis.

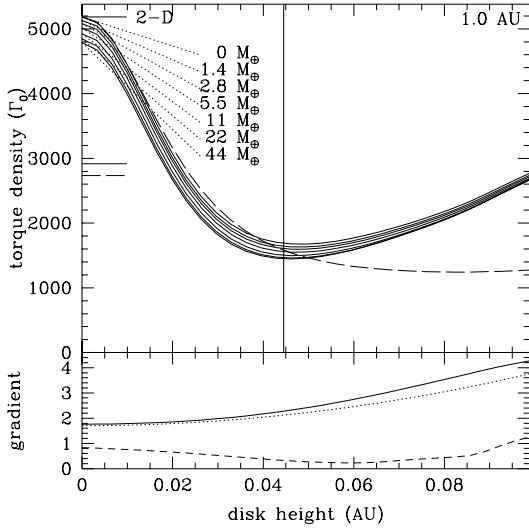


FIG. 3.— Scaled torque density profiles, and density and temperature gradients as a function of height at 1 AU. The vertical line indicates the disk's scale height. (Upper panel): The scaled torque density, in terms of Γ_0 , is plotted versus height from the midplane for a disk with and without a planet, the mass of the planet indicated by the labels. The dashed line indicates the net torque in a vertically isothermal disk at the midplane temperature. The short horizontal lines on left edge of the plot show the total integrated torque for the unperturbed (solid line) and vertically isothermal (dashed line) disk models. (Lower panel): The temperature gradient, l , is plotted as a dashed line. The quantities $[k + 3(\Omega_K/c)^2/2]$ (solid line) and $[k_\sigma + 3/2 + (l|_{z=0})z^2/2h_0^2]$ (dotted line) are also plotted.

torque density for the unperturbed model disk. For comparison, we have plotted the scaled torque density profile for a vertically isothermal disk with $T = T(z=0)$ as a dashed line.

Close to the midplane, the torque density falls off rapidly with z . It then levels off and rises again toward high altitudes. The sharp drop-off occurs because of the dependence on z of the perturbing potential, indicating that the thickness of the

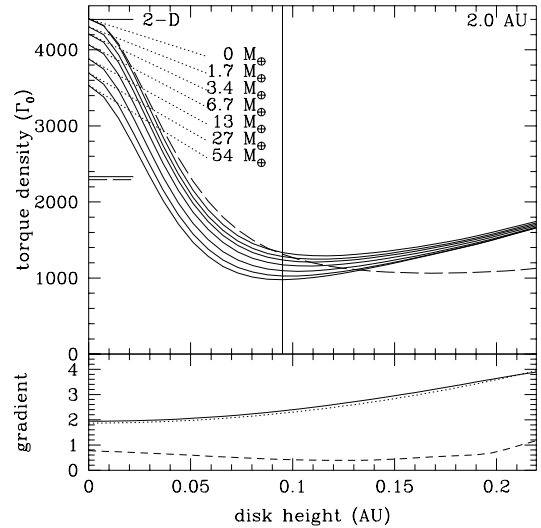


FIG. 4.— Scaled torque density profiles, and density and temperature gradients as a function of height at 2 AU. See Figure 3 for a full description of this plot.

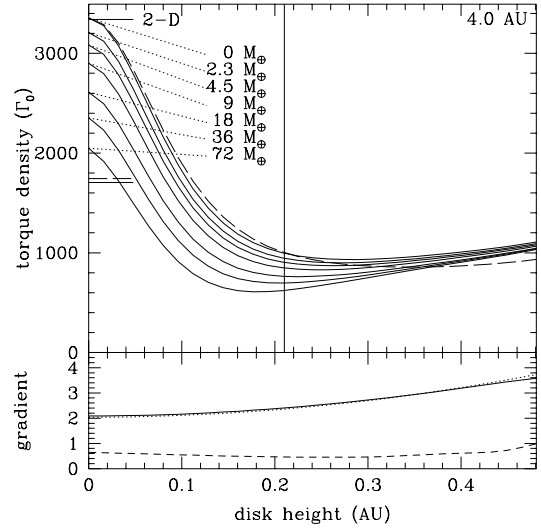


FIG. 5.— Scaled torque density profiles, and density and temperature gradients as a function of height at 4 AU. See Figure 3 for a full description of this plot.

disk does play an important role in diluting angular momentum transfer at Lindblad resonances. All the profiles follow the same basic shape near the midplane, including the vertically isothermal one.

The torque density for the model disk increases at high altitudes above that of the isothermal disk because of several attributes of the disk that all increase the relative differential torque higher in the disk. Firstly, the Lindblad torque scales roughly as c^{-2} (Ward 1986; Korycansky & Pollack 1993) and the vertical temperature minimum roughly corresponds to the photosphere, which is the limit of our integration in z . Secondly, the radial temperature gradient, l , rises slightly between the disk scale height and the photosphere. We plot l versus z as a dashed line in the lower panel in each of Figures 3, 4, and 5. The higher values of l favor torques from the outer Lindblad resonances by shifting their locations, so

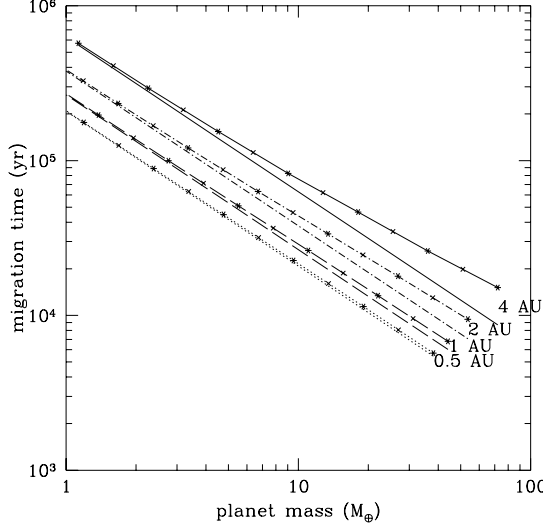


FIG. 6.— Comparison between migration timescales in the disk-planet system in the presence of temperature perturbations and the absence of temperature perturbations. We plot the migration timescale versus planet mass at 0.5 (dotted line), 1 (dashed line), 2 (dot-dashed line) and 4 (solid line) AU, showing the perturbed and unperturbed times as lines with and without points. (The six-pointed stars represent calculated models, the crosses are interpolations for illustration.)

the net torque rises (Ward 1997a). Thirdly, the density gradient, k , is greater than the isothermal density gradient. As shown in equation (4), the location of the resonance is shifted by a factor proportional to $(3z^2/2h^2 + k + l)$. The quantity $[k + 3(z\Omega_K/c)^2/2]$ in the model disk is plotted as a solid line in the lower panel of Figures 3, 4, and 5. For comparison, $[k_\sigma + 3/2 + (l|_{z=0})z^2/2h_0^2]$, which is the equivalent quantity in a vertically isothermal disk, is also plotted as a dotted line. The solid line rises above the dotted line most noticeably at 1 AU in Figure 3, which is also where the rise in the torque density is most significant.

The total integrated net torques at 1 and 2 AU in the model disk are greater than the total torques for an equivalent isothermal disk. This is because the temperature decreases with z up to the photosphere in the model disk, so the density falls off more than in a vertically isothermal disk, as shown in Figure 1. This leads to greater sampling of the torque at the disk midplane relative to the photosphere. As the distance from the star increases, the vertical temperature profile flattens, and the density profile rises relative to the profile of the isothermal disk. Contributions to the total torque from the upper layers rise relative to contributions from the midplane, effectively softening the total torque as a whole, and the total net torque of the model disk falls below that of the isothermal disk.

At 1 AU and inwards, the effect of planet-induced temperature variations are small. However, as the distance increases to 2 and 4 AU, planet-induced temperature variations become more effective at changing the torque from Lindblad resonances. These results are shown in Figure 6, where we plot migration time scales versus planet mass at 0.5, 1, 2, and 4 AU as dotted, dashed, dot-dashed, and solid lines, respectively. The lines with and without points show migration time scales in the model disk with and without considering local temperature perturbations, respectively. At 0.5 AU, the migration timescales are changed very little by the temperature perturbations. Further from the star, the departures from the

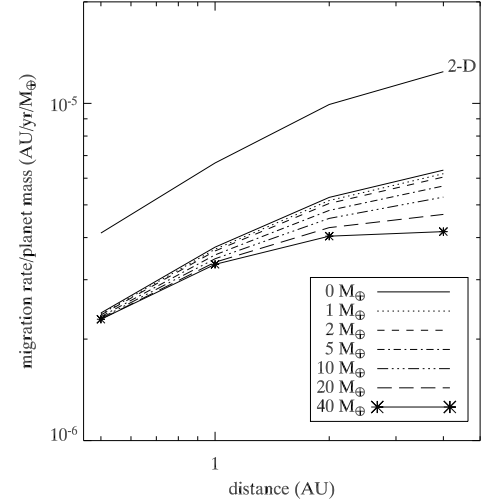


FIG. 7.— Migration rates for the model disk-planet system scaled by the planet mass. The upper solid line labelled “2D” is the migration rates for an equivalent two-dimensional disk using the formulation of Ward (1997a). The lower lines are the migration rates calculated for the full three-dimensional disk including temperature perturbations from a planet with mass indicated in the legend. The solid line, marked $0 M_\oplus$ in the legend, shows migration rates for the disk in the absence of any planet-induced temperature perturbations.

unperturbed disk become more and more pronounced. This is, in part, due to the vertical density profile, which weights the torques at the midplane more heavily at closer distances to the star, as discussed above. But as can be seen from Figures 3, 4, and 5, the torques at the midplane are also more affected with increasing distance. This is because the total optical depth of the disk decreases with distance as the surface density falls off. This increases shadowing and illumination effects at the midplane, which has a greater effect on the net Lindblad torques there.

We re-plot these results in terms of migration rate per Earth mass versus distance from the star in Figure 7. Given the grid of planet distances and masses we have sampled, we interpolate to find the migration rate for selected planet masses and plot the variation of migration rate with distance for different planet masses, as indicated by the different lines. In the absence of perturbations to the disk, the migration rate scales with the mass of the planet, so this is good way to concisely summarize the effects of local temperature variations. Close to the star, even planets at the gap-opening threshold reduce the migration rate by only a few percent. However, as the distance increases, planet-induced temperature variations become more and more effective at lowering the migration rate, up to 43% at 4 AU. For comparison, we also plot the migrations rates for a comparable two-dimensional disk, which gives migration rates of about twice as fast as the unperturbed three-dimensional disk. For this model disk, the overall trend is that planetary migration slows as the planet moves closer to the star rather than staying constant, although this deceleration is not sufficient to keep planets from migrating right into the star.

5. DISCUSSION

Although the density of the disk is highest at the midplane, the contributions to the Lindblad torques at the midplane do not solely determine the total net migration torque. The finite thickness of the disk is also important because it both modifies the perturbing potential and shifts the resonance positions.

For our model disk, we find that including the thickness of the disk reduces the migration rate by about a factor of two from a two-dimensional disk. By comparing the model disk with an equivalent isothermal disk, we find that including the vertical softening of the perturbing potential is, in fact, the primary effect, and that the vertical temperature structure has a modest effect. We show how the torques in these model disks compare to each other in Figure 8. The model disk is shown as a solid line, the two-dimensional disk is the short-dashed line, and the isothermal disk as a dotted line.

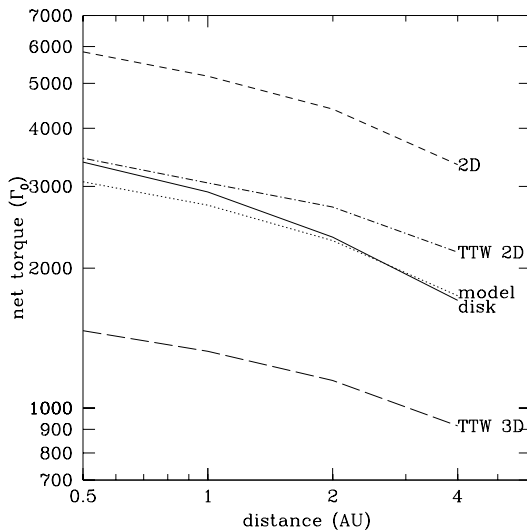


FIG. 8.— Comparison of migration torques between different disk models vs. radius. All disk models have the same midplane density and surface density as the model disk. We show the three-dimensional model disk (solid line), a vertically isothermal model (dotted line), and a two-dimensional disk (short dashed line). We also show for comparison the calculation done by TTW for a three-dimensional (long dashed line) and two-dimensional (dot-dashed) disk.

TTW also find that the net Lindblad torques in their calculation of a three-dimensional isothermal disk are a factor of $\sim 2 - 3$ less than that of the equivalent two-dimensional disk. These torque calculations are also plotted in Figure 8 as a long dashed line for the three-dimensional disk and a dot-dashed line for the two-dimensional disk. While there is a mismatch between the TTW models and our model disk, the results are still qualitatively the same in showing how including the vertical structure of the disk affects the total torque on the planet.

Planet-induced temperature variations can reduce the migration rate relative to that of the unperturbed disk by up to a factor of about 2 for planets at the gap-opening threshold at around 4 AU. Migration rates are less affected closer to the star because of increased viscous heating at the midplane. In general, the midplane of the disk contributes most to the resonant torques since temperature variations are minimal both because of the high optical depth to the stellar irradiation and viscous heating at the midplane. Viscous heating and stellar irradiation behave as $r^{-3/4}$ and $r^{-1/2}$, respectively, so viscous heating increases faster with decreasing radius than stellar ir-

radiation. Midplane temperature perturbations are therefore washed out by viscous heating closer to the star. This is why the presence of a planet has little effect at 0.5 AU, but is highly effective at 4 AU.

The results of Menou & Goodman (2004) also show that the thickness of a three-dimensional disk accounts for a significant increase in migration timescales over those of two-dimensional disks. They consider an α -disk model similar to ours, and find that opacity changes in the disk create local regions of increased migration timescale, or decreased migration rate, because of local variations in the temperature gradient. The spikes in the migration timescale that result from local changes in the temperature gradient close to the star ($\lesssim 1$ AU) may be softened by shadowing effects, since these local effects may dominate over the large-scale temperature gradient.

As a planet migrates inward, the gap-opening threshold mass decreases, so the planet may begin to open a gap and undergo Type II migration rather than Type I migration. This is a feature of any disk model with a flared structure, where h increases faster than r . The gap-opening threshold is where $r_H \equiv (m_p/3M_*)^{1/3}r = h$. Rewriting this equation, the gap-opening threshold mass is

$$m_p = 3M_* \left(\frac{h}{r} \right)^3. \quad (31)$$

If $d \log h / d \log r > 1$, then the gap-opening mass increases with r . In Type II migration, the planet remains fixed with respect to the disk instead of moving through it, as in Type I migration. As the disk is accreted onto the star, the planet moves with it in the viscous time scale. This is an altogether different mechanism for slowing migration. However it still suffers from the problem that as long as the disk exists, the planet will migrate together with the disk and could still fall into the star.

6. SUMMARY AND CONCLUSIONS

We have analyzed the effect of local disk temperature variations on Type I migration rates of planets embedded in protoplanetary disks. We include both the vertical structure of the disk as well as temperature perturbations caused by the presence of the planet itself.

In comparison to the results of Ward (1997a) for a two-dimensional disk model, the primary difference in migration rates is caused by including the vertical thickness of the disk. This is because the perturbing potential is diluted by the vertical distance from the midplane. When we integrate the total torque at Lindblad resonances over the vertical extent of the disk, we find that this reduces the migration rate by about a factor of two. This is consistent with calculations by TTW, who find that the vertical dependence of the perturbing potential reduces migration rates by a factor of $\sim 2 - 3$ in their model disk.

We estimate the effect of including the vertical temperature and density profile of the model disk by comparing it to an equivalent vertically isothermal disk and find that the effect on the migration rates is modest. This is in part because the torque is weighted by disk density, which is highest at the midplane, and also because of the rapid decrease in torque density with disk height. Therefore disks with the same midplane temperature and density profiles will yield similar migration rates.

When we include the effects of radiative transfer on the perturbation caused by the planet on the disk, we find that

the resulting temperature perturbations can further decrease the migration rate by up to about a factor of two, depending on the planet's mass and position. As the planet increases in mass, so does the temperature variation, which results in a general decrease in the migration rate. The effect is more prominent in planets further from the star, because viscous heating decreases faster than stellar illumination with increasing distance. Viscous heating evens out temperature variations, reducing their impact on Lindblad torques. Thus, the planet at the gap-opening threshold at the farthest distance in our sample is the most effective at reducing its own migration rate.

Our calculation of migration torques given the temperature structure in the photosphere of the disk shows a limiting case, since we assume that only the local temperature of the disk is relevant, and that the azimuthal dependence on temperature is unimportant. This is justified by the fact that the perturbing potential is strongest closest to the planet, but in principle the azimuthal variation of the temperature could dilute the effect of local temperature variations on migration rates.

Another limitation of our planet-disk model is that we have not considered the non-linear perturbation to the density struc-

ture within a few Hill radii of the protoplanet. Since the tidal torques from Lindblad resonances scale with disk density, this effect may be very important. Numerical simulations universally show that spiral structure develops quickly around planets embedded in disks. Radiative transfer from stellar illumination upon these structures can affect the planet and disk both directly through heating, and indirectly by changing the positions and strengths of the Lindblad resonant torques.

Still, our model puts interesting constraints on the effect of the temperature and density structure on Type I migration. We have shown that shadowing and illumination at the surface of a protoplanetary disk can slow migration. If the perturbations are large enough, they might be able to halt or even reverse Type I migration, and save planet embryos from the “Shiva catastrophe” (Ward 1997b). Perhaps this can explain why the frequency of giant planets around solar-type stars is relatively high, despite the short timescales predicted for Type I migration.

We thank Kristen Menou and our anonymous referee for their helpful comments in the preparation of this paper.

REFERENCES

Abramowitz, M., & Stegun, I. A. 1972, *Handbook of Mathematical Functions* (Handbook of Mathematical Functions, New York: Dover, 1972)

Artynowicz, P. 1993a, *ApJ*, 419, 166

—. 1993b, *ApJ*, 419, 155

Bate, M. R., Lubow, S. H., Ogilvie, G. I., & Miller, K. A. 2003, *MNRAS*, 341, 213

Calvet, N., Patino, A., Magris, G. C., & D’Alessio, P. 1991, *ApJ*, 380, 617

D’Alessio, P., Calvet, N., Hartmann, L., Lizano, S., & Cantó, J. 1999, *ApJ*, 527, 893

D’Alessio, P., Canto, J., Calvet, N., & Lizano, S. 1998, *ApJ*, 500, 411

Goldreich, P., & Tremaine, S. 1980, *ApJ*, 241, 425

Jang-Condell, H., & Sasselov, D. D. 2003, *ApJ*, 593, 1116

—. 2004, *ApJ*, 608, 497

Kley, W. 1999, *MNRAS*, 303, 696

Kley, W., D’Angelo, G., & Henning, T. 2001, *ApJ*, 547, 457

Korycansky, D. G., & Pollack, J. B. 1993, *Icarus*, 102, 150

Lubow, S. H., & Ogilvie, G. I. 1998, *ApJ*, 504, 983

Menou, K., & Goodman, J. 2004, *ApJ*, 606, 520

Nelson, R. P., & Papaloizou, J. C. B. 2004, *MNRAS*, 350, 849

Shakura, N. I., & Sunyaev, R. A. 1973, *A&A*, 24, 337

Takeuchi, T., & Miyama, S. M. 1998, *PASJ*, 50, 141

Tanaka, H., Takeuchi, T., & Ward, W. R. 2002, *ApJ*, 565, 1257

Ward, W. R. 1986, *Icarus*, 67, 164

—. 1988, *Icarus*, 73, 330

—. 1997a, *Icarus*, 126, 261

—. 1997b, *ApJ*, 482, L211